

Green Ironmaking Industry: Production of Iron Pellets Using Lime Sludge

Lucio Rosso Neto^{a*} , Carlos Henrique Borgert^a, José Roberto de Oliveira^b,

Felipe Fardin Grillo^b , Gabriel Valério Pereira Manfredi^c, Jorge Luis Coletti^c,

Denise Croce Romano Espinosa^c, Jorge Alberto Soares Tenório^c, David Batista Gesuino^a,

Tiago Elias Allievi Frizon^d, Eduardo Junca^a 

^aUniversidade do Extremo Sul Catarinense, Laboratório de Metalurgia e Tratamento de Resíduos Industriais (LAMETRI), Programa de Pós-Graduação em Ciência e Engenharia de Materiais, Av. Universitária, 1105, Bairro Universitário, 88806-000, Santa Catarina, SC, Brasil.

^bInstituto Federal de Educação Ciência e Tecnologia do Espírito Santo, Departamento de Engenharia Metalúrgica e de Materiais, Av. Vitória, 1729, Jucutuquara, 29040-780, Vitória, ES, Brasil.

^cUniversidade de São Paulo, Escola Politécnica, Departamento de Engenharia Química, Laboratório de Reciclagem, Tratamento de Resíduos e Extração, Av. Prof. Lineu Prestes, 580, Butantã, 05508-000, São Paulo, SP, Brasil.

^dUniversidade Federal de Santa Catarina, Departamento de Energia e Sustentabilidade, Rua Gov. Jorge Lacerda, 3201, Araranguá, 88906-072, SC, Brasil.

Received: April 20, 2022; Revised: December 12, 2022; Accepted: December 15, 2022

The use of alternative raw materials is essential for establishing a circular economy in the mineral and ironmaking sectors. Therefore, this study investigates the potential of lime sludge as fluxing material during pelletization and proposes an alternative route for the usage of waste. The pellets were manufactured with different binary basicity values (CaO/SiO₂) (0.15–0.45) and bentonite (0.5–0.7 wt%) and fixed carbon (0.5–1.1 wt%) contents. The results demonstrated that lime sludge has significant potential for application in pelletization. Pellet quality was evaluated using drop number, mechanical strength, tumble index, porosity, and kinetic analyses. Pellets with the optimal composition using lime sludge withstood 3.6 drops/pellet, a tumble test of 1.57 wt.%, and a mechanical strength test of 214.83 kgf/pellet and exhibited a porosity of 31.28%. Lime sludge did not influence the reducibility of the iron-ore pellets. In the temperature range of 800–900 °C, the reaction was controlled by diffusion, with E_a between 179.89 and 233.10 kJ/mol.

Keywords: Circular economy, Solid waste, Lime sludge, Ironmaking.

1. Introduction

The global production of crude iron reached 1877.3 million tons in 2020. Brazil is the 9th leading producer of crude steel in the world, accounting for 31.4 million tons. According to Rath et al.¹, approximately 70% of the total steel in the world is produced in blast furnaces (BFs). The raw materials for these reactors include the iron ore (sinter, iron-ore pellets or lump), coke (energy source), and lime (fluxing material). Estimates indicate an increase in the steel production of approximately 2.8 million of tons by 2050, which consequently entails an increased demand for raw materials. The iron-ore pellet is an essential feed in the BF because of its uniform particle size distribution (9–16 mm) and chemical composition^{2,3}. The pelletization process uses a fine powder of iron ore (lesser than 0.15 mm; as the source of iron), lime (fluxing material), and coal (solid fuel) as raw materials⁴.

The company Vale reported a production of 29.676 million tons of iron-ore pellets from Brazilian plants in 2020⁵⁻⁷. The increase in the global demand for steel also increases the

demand for iron-ore pellets and, consequently, the demand for inputs for this production sector. Other issues include the price increase and finite sources of raw materials available for ironmaking plants, thereby motivating the use of sustainable alternative materials. Norouzi et al.⁸ mentioned circular economy (CE) as an industrial ecosystem and symbiosis and a cleaner production system that involves circular material flows for manufacturing systems. The concept of CE proposes that a waste generated from an industrial sector may be used as the raw material for another. According to Dishwar and Sinha⁹, the concept of CE involves a regenerative model to minimize the inputs (resources) and waste in any form of leakage. In this regard, the academic community can contribute toward this aim by investigating the potential applications of a given residue or developing clean technologies.

Lime sludge, which is a waste material generated by the pulp and paper industry, is mainly disposed in landfills located near the factories, which demand high costs for implementation and maintenance. According to IBÁ¹⁰, Brazil produced 10.5 million tons of paper in 2019. Consider that

*e-mail: luciorosso@Outlook.com

each ton of paper generates approximately 1.63 tons of lime sludge¹¹, an estimated 16.8 million tons of lime sludge was generated in 2019. One chemical characteristic of lime sludge is that it is a CaCO₃-rich material. Phanikumar and Raju¹² found that lime sludge contained 50 wt% of CaO with a loss upon ignition of 40 wt% (from the decomposition of calcium carbonate). The authors also determined other components, such as 7 wt% of SiO₂ and lesser contents of Al₂O₃, Na₂O, and Fe₂O₃. Considering its physical characteristics, lime sludge has particle sizes of 12.20 (D10), 36.66 (D50), and 68.48 μm (D90)¹³. Therefore, the lime sludge presents potential application in the process of iron ore pelletization as a replacement for limestone as fluxing material.

Changes in the mechanical behavior of iron-ore pellets are due to changes in the characteristics of the inputs. For example, the amount of limestone required to produce the pellets depends on the production sector and quality of the inputs. Limestone is added in the mixture to adjust the binary basicity (CaO/SiO₂) because increasing the binary basicity in the pellets may endow benefits such as weather resistance and early slag formation⁹. Guo et al.¹⁴ studied values of binary basicity between 0.2–1.2 (using limestone) to produce iron-ore pellet using high-grade iron concentrates and found that a binary basicity exceeding 1.0 produced a good reduction swelling index. Meanwhile, Umadevi et al.¹⁵ determined that the binary basicity for producing iron-ore pellets should be 0.33. Santos et al.⁴ indicated that the maximum mechanical performance of the iron-ore pellet was observed at a basicity of 0.45. Najafabadi et al.² studied the abrasive damage of industrial iron-ore pellets with a binary basicity of 0.21.

These differing findings suggest that studies are necessary to understand the alterations caused by the use of lime sludge on the characteristics of the resulting iron-ore pellets. In addition, the correct proportion of inputs (such as lime sludge, coal, and bentonite) should be determined to optimize the productive process and consequently decrease both the amount of raw material and environmental impacts. Therefore, this study aims to produce iron-ore pellets using lime sludge as fluxing material to create a symbiosis between the waste generated in the pulp and paper industry with the iron-ore pelletizing process, thereby promoting a manufacturing system with a circular material flow.

2. Experimental

2.1. Raw materials characterization

Table 1 summarizes the chemical composition of the inputs used to produce the iron-ore pellets. The chemical composition of the hematite iron ore was provided by a Brazilian company that supplied the sample. The chemical compositions of coal ash, bentonite, dolomite, and lime sludge were determined using X-ray fluorescence (Axios Max Panalytical)⁴.

The source of carbon was a mineral coal from Santa Catarina States, Brazil. The contents of fixed carbon, volatile material, and ash were determined on an STA 449F3 NETZSCH thermobalance in two steps. First, thermogravimetric analysis was conducted under inert atmosphere (N₂) at a flow of 40 mL/min. The temperature range was 30–1000 °C, and the heating rate was 5 °C/min. The mass lost in this step was the volatile material content. The remaining mass was subjected to another warm-up program under O₂ atmosphere at a flow of 40 mL/min and within a temperature range of 30–1000 °C. Fixed carbon accounted for the mass loss in this step. The remaining mass in the crucible was the ash content.

Mineral coal was milled in a Servitech CT-242 ball mill to obtain particle size lesser than 200# (74 μm) for producing the iron-ore pellets. In addition, particle sizes of the lime sludge, dolomite, and iron ore were analyzed using laser diffraction (CILAS 1064) with water as liquid.

2.2. Production of iron-ore pellets

The mixtures for the pelletizing process were defined by a 2³+2 experimental design, with three variables and two central points. The variables were binary basicity (0.15–0.45) and percentages of bentonite (0.5%–0.7%) and fixed carbon (0.5%–1.1%), which were denoted by symbols Ba, B, and C, respectively. The subscribed numbers indicate the value of that variable in the mixture. For example, Ba_{0.3}-C_{0.8}-B_{0.6} refers to a mixture with a binary basicity of 0.3 and percentages of fixed carbon of 0.8% and bentonite of 0.6%.

The raw materials were weighed and manually homogenized in a closed plastic bag and then pre-moistened with 6 wt% (wet basis) of water. Pelletization was conducted in a

Table 1. Chemical compositions of the iron ore, dolomite, and lime sludge used as inputs for producing iron-ore pellets.

Component (wt%)	Iron ore	Coal ash	Bentonite	Dolomite	Lime sludge
Al ₂ O ₃	0.73	26.81	20.97	0.01	0.13
BaO	-	-	-	-	0.02
CaO	0.07	1.72	2.41	32.51	54.85
Fe total	65.39	3.54	4.2	0.06	0.17
FeO	1.3	-	-	-	-
MnO	0.08	-	-	-	0.03
MgO	0.08	0.81	3.05	17.78	0.29
K ₂ O	0.01	2.83	0.48	0.02	0.09
Na ₂ O	0.01	0.5	3.41	0.03	2.64
SiO ₂	1.86	62.12	65.21	3.88	1.68
TiO ₂	-	1.18	0.27	-	-
SO ₃	-	0.49	-	-	-
Loss on ignition	-	-	-	45.71	40.07

pelletizing disk with a diameter of 602 mm, 50° of inclination, and rotation speed of 30 rpm. The moisture was gradually added into the pelletizing disk, and water was sprayed on the moisture using a spray bottle. The mass of water sprayed was to obtain a final pellet moisture of 9 wt%.

The pellets were separated using 9 and 16 mm sieves. Approximately 2000 g of the pellets were fired at 1300 °C for 10 min in a muffle furnace at the heating rate of 10 °C/min.

2.3. Determination of Pellet Quality

After the pelletizing process, 10 green pellets (without cracks) with diameters between 9 and 16 mm were subjected to the drop test. The pellets were allowed to free-fall from a height of 45 cm onto a flat surface. The drop number was the maximum number of times the pellets maintained their integrity (absence of cracks).

The mechanical compressive strength of the dry pellets was determined using 10 dried pellets (muffle furnace) at 105 °C for 24 h. The mechanical compressive strength was evaluated using a universal testing machine, model EMIC DL-1000, equipped with a load cell of 1000 kgf at a speed of 15 mm/min.

The fired pellets were used in the tumble, compressive strength, and porosity tests. The tumble test was adapted from standard ISO 3271:2015—Determination of the tumble and abrasion indices. This test involved placing 2000 g of pellets (with diameters of 9–16 mm) into an alumina jug with diameter and length of 176 and 271 mm, respectively, for 200 rotations at a rotational speed of 43 rpm. The rotational speed adopted in this test was calculated to be the same as that used in ISO 3271:2015¹⁶ to promote a similar fall regime of the pellets inside the jar. The tumble index was the mass of fine particles less than 4 mm.

The compressive strength of the fired pellets was determined using the same universal testing machine (DL 10000, EMIC) described previously. A 1000 kgf loadcell was used at a speed of 15 mm/min (ISO 4700:2015)¹⁷. The compressive strength was determined from the average results of the 10 pellets.

To determine the porosity of the pellets, 20 fired pellets were washed in running water for 10 min. The pellets were then dried at 105 °C for 24 h in a muffle furnace to determine the initial pellet mass (P_s). In the subsequent step, the pellets were submerged in a 100 °C water bath for 5 h. Afterward, excess water was removed using paper to determine the mass of wet pellets (P_m). A specific mass of water of 1 g/cm³ was adopted. Therefore, the pore volume of the pellets (V_{po}) was determined using Equation 1.

$$V_{po} = P_m - P_s \quad (1)$$

The mass of a 500 mL volumetric flask (P_b) with deionized water up to the meniscus was measured. The wet pellets were placed into the volumetric flask, and the volume of water was adjusted to the meniscus to determine the mass of the set (P_{bp}) (volumetric flask + deionized water + wet iron-ore pellets). The volume of the pellets (V_{pe}) was determined using Equation 2, and the porosity was calculated using Equation 3.

$$V_{pe} = P_b - (P_{bp} - P_m) \quad (2)$$

$$\%_{poros} = (V_{po} / V_{pe}) \times 100 \quad (3)$$

Optical microscopy (Olympus, model BX41RF / LED) images were taken to analyze the pore distribution in the fired pellets. The pellets were embedded with cold curing resin and sanded with a series of sandpaper (80, 200, 400, and 800 grit) until the core was revealed.

Statistical analysis demonstrates the influence of independent variables (Ba, C, and B) on the fired iron-ore pellets (mechanical strength of the fired pellet and porosity). The trial Statistica software was used with a 95% confidence interval ($\alpha = 0.05$).

2.4. Analysis of computational thermodynamics

Computational thermodynamics analysis was conducted to investigate the phases formed during the firing step. The simulation was performed in the temperature range of 800–1300 °C using the Thermocalc software adopting the SLAG 3 database. Simulation was conducted for the mixtures Ba_{0.3}-C_{1.1}-B_{0.7} and Ba_{0.45}-C_{0.5}-B_{0.7}, as they exhibited the highest mechanical strength. The compositions of the mixtures (Table 2) were calculated using mass balance from the chemical composition of the raw materials.

2.5. Kinetic investigation

Pellet reduction tests were performed on a Netzch STA 449F1 thermogravimetric analyzer using pellets with a diameter of 10 ± 0.3 mm. The kinetic investigation was conducted in the temperature range of 700–1100 °C. The pellet was heated to 700 °C at a heating rate of 10 °C/min under 40 mL nitrogen flow. Thereafter, isotherms were programmed at every 50 °C intervals in the temperature range between 700 and 1100 °C, with an isothermal time of 15 min. Under isothermal conditions with CO as reducing gas, tests were conducted at flow rates of 50, 100, 150, and 200 mL/min to investigate the external gas diffused into pellets through the gas-phase boundary layer. Heating between consecutive isotherms was performed under nitrogen atmosphere (40 mL/min) at a heating rate of 10 °C/min to prevent reduction reaction occurring outside the isothermal conditions. A reduction test using 15 mm-diameter pellets was conducted to investigate the influence of diffusion on the reduction process.

Based on Equation 4, the reacted fraction (α) was determined from the mass loss obtained in the thermogravimetric tests under a CO flow of 150 mL/min, according to Equation 4¹⁸. The kinetic studies were conducted using the analysis presented in Equation 5¹⁹, in which $f(\alpha)$ is the function that describes the controlling mechanism (Table 3), and k is the velocity constant that obeys Arrhenius law (Equation 6)²⁰.

$$\alpha = \frac{m_0 - m_T}{m_0 - m_f} \quad (4)$$

$$\frac{d\alpha}{dt} = k(T) \cdot f(\alpha) \quad (5)$$

$$k = A \cdot \exp\left(-\frac{E_a}{RT}\right) \quad (6)$$

Table 2. Chemical composition of the iron-ore pellets obtained for mass balance used in thermodynamic simulations.

Mixtures	Components (wt%)								
	Al ₂ O ₃	CaO	Fe ₂ O ₃	MnO	MgO	K ₂ O	Na ₂ O	SiO ₂	FeO
Ba _{0.3} -C _{0.8} -B _{0.6}	1.05	0.81	93.90	0.08	0.11	0.04	0.07	2.69	1.25
Ba _{0.3} -C _{0.8} -B _{0.6}	1.05	0.81	93.90	0.08	0.11	0.04	0.07	2.69	1.25
Ba _{0.3} -C _{1.1} -B _{0.7}	1.14	0.88	93.48	0.08	0.11	0.05	0.08	2.93	1.24
Ba _{0.15} -C _{0.5} -B _{0.5}	0.95	0.37	94.68	0.08	0.10	0.03	0.04	2.46	1.27
Ba _{0.15} -C _{0.5} -B _{0.7}	0.99	0.39	94.49	0.08	0.11	0.03	0.05	2.59	1.27
Ba _{0.15} -C _{1.1} -B _{0.5}	1.10	0.42	94.12	0.08	0.10	0.04	0.05	2.81	1.25
Ba _{0.15} -C _{1.1} -B _{0.7}	1.14	0.44	93.92	0.08	0.11	0.04	0.06	2.94	1.25
Ba _{0.45} -C _{0.5} -B _{0.5}	0.95	1.11	93.95	0.08	0.10	0.03	0.08	2.45	1.25
Ba _{0.45} -C _{0.5} -B _{0.7}	0.99	1.16	93.71	0.08	0.11	0.03	0.09	2.58	1.25
Ba _{0.45} -C _{1.1} -B _{0.5}	1.10	1.26	93.28	0.08	0.11	0.05	0.09	2.80	1.23
Ba _{0.45} -C _{1.1} -B _{0.7}	1.14	1.32	93.04	0.08	0.11	0.05	0.10	2.92	1.23

where m_0 is the initial mass; m_f is the final mass; m_T is the mass at temperature T ; A is the pre-exponential factor; R is the ideal gas constant; T is the temperature, and E_a is the activation energy.

The control kinetic model was defined based on the linear trend of the relationships of da/dt vs $f(\alpha)$ and $\ln(k)$ vs $1/T$ higher than 0.9. The E_a was determined from the relationship of $\ln(k)$ vs $1/T$, where E_a was calculated using the slope. In addition, values of E_a between 13.4 and 246 kJ/mol were considered acceptable²¹⁻²³.

Reduction tests were interrupted at the end of the 700 and 800 °C isotherms for characterization using X-ray diffraction (XRD) and scanning electron microscopy (SEM). XRD was conducted on a Miniflex 300 Rigaku diffractometer with a Cu K α tube ($\lambda = 1.5418 \text{ \AA}$), with a scan range of 20–80°, step width of 0.02°, and time of 5 s. A TA Phenom ProX scanning electron microscope with energy-dispersive spectroscopy was used.

3. Results and Discussion

3.1. Material characterization

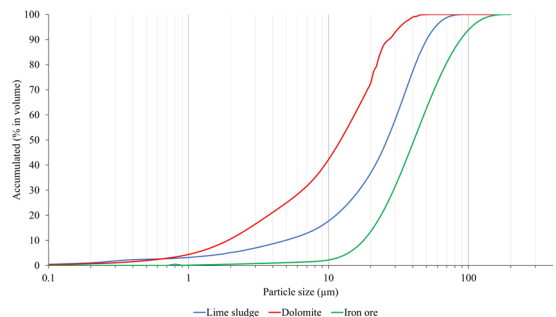
Size analysis results (Figure 1) show that lime sludge had 90% of particles sizes less than 50.25 μm , 50% less than 26.14 μm , and 10% less than 4.91 μm . Dolomite presented 90% of particle sizes less than 29.36 μm , 50% less than 12.19 μm , and 10% less than 1.9 μm . The iron ore had 90% of particle sizes less than 87.30 μm , 50% less than 40.80 μm , and 10% less than 17.75 μm .

3.2. Iron Ore Pellet Quality

Figure 2 demonstrates that the drop test results of iron-ore pellets containing lime sludge ranged from 2.0 ± 0 (Ba_{0.3}-C_{0.8}-B_{0.6}) to 3.6 ± 0.843 drops/pellet (Ba_{0.45}-C_{0.5}-B_{0.7}). The result for pellets containing limestone (Ba_{0.3}-C_{1.1}-B_{0.7}) was 3.4 ± 0.516 drops/pellet, indicating that lime sludge increased this index by up to 5.5%. Sivrikaya and Arol²⁴ mentioned that the minimum value required by the pellets in the drop test is 4. Therefore, considering the standard deviation, the results for the Ba_{0.45}-C_{0.5}-B_{0.7} pellets slightly exceeded the limit.

Table 3. Kinetic models for the gas–solid reaction.

Mechanisms	Symbol	$f(\alpha)$
Phase boundary controlled	R2	$(1-\alpha)^{1/2}$
Phase boundary controlled	R3	$(1-\alpha)^{1/3}$
One-dimensional diffusion	D1	$1/\alpha$
Two-dimensional diffusion	D2	$\frac{1}{-\ln(1-\alpha)}$
Three-dimensional diffusion (Jander)	D3	$\frac{(1-\alpha)^{2/3}}{1-(1-\alpha)^{1/3}}$
Three-dimensional diffusion (Ginstling-Brounshtein)	D4	$\frac{1}{[(1-\alpha)^{-1/3} - 1]}$
Two-dimensional nucleation	A2	$(1-\alpha)[- \ln(1-\alpha)]^{1/2}$
Three-dimensional nucleation	A3	$(1-\alpha)[- \ln(1-\alpha)]^{2/3}$

**Figure 1.** Size analysis of lime sludge, dolomite, and iron ore used to produce iron-ore pellets.

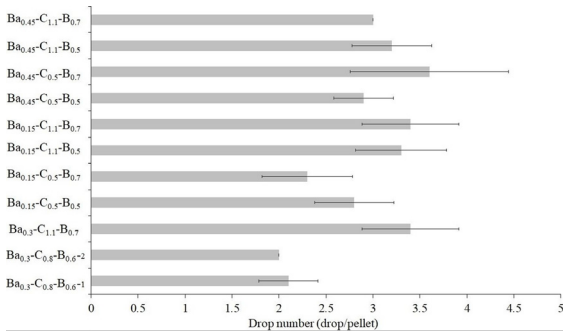


Figure 2. Influence of the composition on drop number of the green iron-ore pellets.

According to Forsmo²⁵ the initial resistance of green pellets is provided by the interaction of water with the binding agent (bentonite). In addition, lime sludge contains a higher percentage of fine particles than limestone, which tends to increase the capillary pressure when in contact with water, thereby increasing pellet plasticity^{26,27}.

Figure 3 shows the tumble test results of the fired iron-ore pellets. The results ranged between 1.28% (Ba_{0.45}-C_{1.1}-B_{0.7}) and 5.98% (Ba_{0.15}-C_{1.1}-B_{0.7}). The midpoints (Ba_{0.3}-C_{0.8}-B_{0.6}) showed tumble index values of approximately 1.4%. The pellet containing dolomitic limestone (Ba_{0.3}-C_{1.1}-B_{0.7}) presented a tumble index of 2.09%. Umadevi et al.¹⁵ mentioned that pellets with higher basicity generally exhibit better tumble index because of the increase in the content of the liquid phases formed during the fire step, which improves bonding between the iron-ore grains²⁸.

The results of mechanical strength testing of dry pellets (Figure 4) containing lime sludge varied from 1.07 (Ba_{0.3}-C_{0.8}-B_{0.6}) to 3.20 kgf (Ba_{0.45}-C_{0.5}-B_{0.7}). The mechanical strength of dry pellets with dolomite (Ba_{0.3}-C_{1.1}-B_{0.7}) was 1.75 kgf. According to Sivrikaya and Arol²⁴ the required mechanical strength of dry pellets is between 1.0 and 2.0 kgf. The results demonstrate that increasing the content of fixed carbon also increases the mechanical strength of the dried pellets. Pellets Ba_{0.45}-C_{0.5}-B_{0.7} and Ba_{0.45}-C_{1.1}-B_{0.7} (with the same binary basicity and bentonite content and different fixed carbon contents) reached mechanical strengths of 3.2 and 1.5 kgf, respectively. The same behavior was observed in pellets Ba_{0.15}-C_{0.5}-B_{0.7} and Ba_{0.15}-C_{1.1}-B_{0.7}, which achieved mechanical strengths of 1.58 and 1.5 kgf, respectively. Notably, increasing the binary basicity increases the mechanical strength.

Figure 5 shows that the compressive strength of the fired pellets ranges from 72.5 (Ba_{0.15}-C_{1.1}-B_{0.7}) to 214.8 kgf (Ba_{0.45}-C_{0.5}-B_{0.7}). The pellets produced with dolomite (Ba_{0.3}-C_{1.1}-B_{0.7}) exhibits a compressive strength of 150.5 kgf. Pellet Ba_{0.45}-C_{0.5}-B_{0.7} reached the highest mechanical strength because of the highest binary basicity index, which increased the content of CaO. The statistical analysis of variance (ANOVA) results (Table 4) demonstrate that only binary basicity presented a *p*-value less than 0.05 (0.013). Therefore, at 95% reliability, binary basicity influences the mechanical strength of the fired iron-ore pellets. The Pareto charts (Figure 6) show that increasing binary basicity increases the mechanical strength of the pellets, indicating a higher

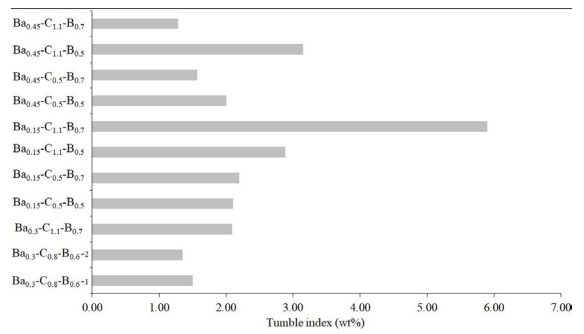


Figure 3. Influence of the composition on tumble index of the fired iron-ore pellets.

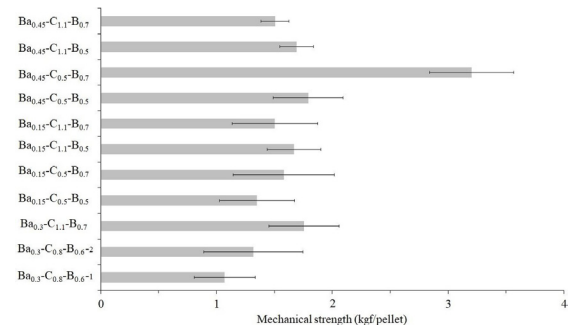


Figure 4. Influence of composition on the mechanical strength of the dried iron-ore pellets.

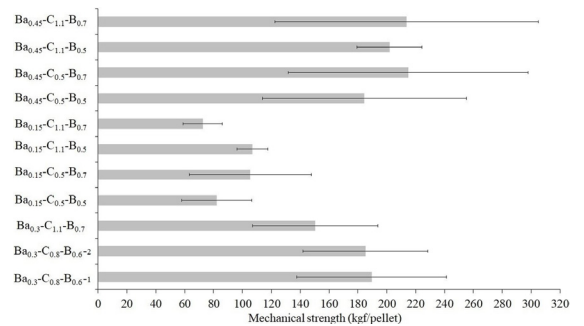


Figure 5. Influence of composition on the mechanical strength of the fired iron-ore pellets.

Table 4. Statistical analysis results for the mechanical strength of the fired iron-ore pellets.

	Degree of Freedom	F-value	p-value
Binary basicity (1)	1	249.73	0.01
Fixed carbon (2)	1	0.07	0.82
Bentonite (3)	1	1.29	0.37
1 by 2	1	0.75	0.48
1 by 3	1	3.55	0.20
2 by 3	1	7.00	0.12
Error	3	-	-

content of calcium carbonate in the composition of the pellets; with the high content of calcium carbonate, calcium aluminum silicate phase forms at a low melting temperature, thereby increasing the content of the liquid phase in the pellet (Figure 7). The thermodynamic simulation also indicates that pellet $Ba_{0.45}-C_{0.5}-B_{0.7}$ reached a liquid-phase value of 8.06 wt%, while pellet $Ba_{0.3}-C_{1.1}-B_{0.7}$ formed 7.48 wt% liquid phase at 1300 °C, indicating that the increasing the binary basicity of the pellets also increases the liquid content during the firing step. Bonding between iron-ore particles originates from the liquid phases formed during the firing step. Consequently, increasing the amount of liquid phase also enhances the mechanical strength of the pellets^{27,29,30}.

Figure 8 shows that the porosity ranges from 29.7% ($Ba_{0.45}-C_{1.1}-B_{0.7}$) to 38.1% ($Ba_{0.15}-C_{1.1}-B_{0.5}$). The pellets produced with dolomite reached a porosity of 33.8%. Pellets with lower binary basicity showed higher porosity because of the decrease in formed liquid phases, which promote the binding between iron-ore grains, during the firing step³¹.

ANOVA results (Table 5) demonstrate that with 95% accuracy, binary basicity and bentonite content exert statistically

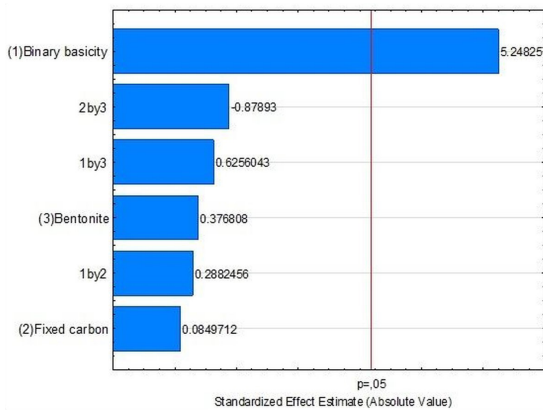


Figure 6. Pareto charts of the mechanical strength of the fired iron-ore pellets.

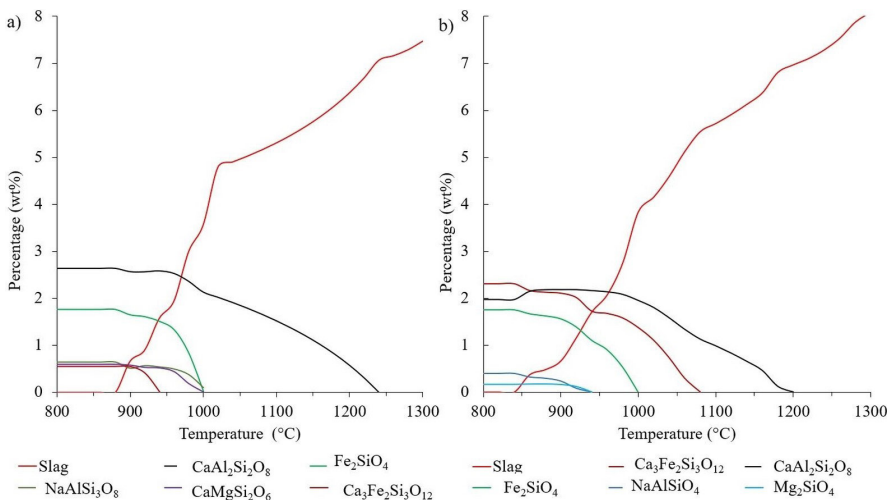


Figure 7. Thermodynamic simulation of the iron-ore pellets. a) Pellet $Ba_{0.45}-C_{0.5}-B_{0.7}$ and b) pellet $Ba_{0.3}-C_{1.1}-B_{0.7}$.

significant effects on porosity, with p -values of 0.001 and 0.007, respectively. The surface graphs (Figure 9) show that the highest porosity value was reached at the lowest binary basicity and bentonite content. Table 5 also exhibit statistical significance (p -value of 0.030) for the interaction between binary basicity and fixed carbon on porosity. These parameters affect the amount of liquid phase formed during the firing step, which alters the porosity. As previously mentioned, increasing the binary basicity increases the amount of liquid phase formed during the firing step, which decreases porosity. Meanwhile, increasing the fixed carbon results in pellets with higher content of volatiles, which lead the carbon combustion prior to the pellet firing step³². Consequently, at 1300 °C, the temperature may not be uniform for all pellet section; thus, the amount of liquid phase formed inside the pellet decreases, while the porosity increases. Therefore, the increase in fixed carbon content associated with the decrease in binary basicity tends to increase porosity, whereas the decrease in fixed carbon content combined with the increase in binary basicity tends to decrease pellet porosity.

3.3. Kinetic investigation

Pellet $Ba_{0.45}-C_{0.5}-B_{0.7}$ was used for kinetic investigation. Figure 10a shows the effect of reducing gas (CO) flow on the reduction rate of iron-ore pellets. The total mass loss in all tests reached approximately 28 wt%. Stabilization of the

Table 5. Results of the statistical analyses for the porosity of the fired iron-ore pellets

Factor	Degree of Freedom	F-value	P-value
(1) Binary basicity	1	442.512	0.001
(2) Fixed carbon	1	0.044	0.847
(3) Bentonite	1	43.339	0.007
(1) by (2)	1	15.097	0.030
(1) by (3)	1	7.510	0.071
(2) by (3)	1	1.545	0.302
Error	3	-	-

loss mass curve at the end means that all of the iron oxide is reduced to iron. Increasing the flow of reducing gas in the range of 50–150 mL/min also increases the reduction rate, indicating that the reaction is limited by the diffusion of the external gas through the boundary layer. Increasing

the reducing gas flow from 150 mL/min to 200 mL/min did not influence the reaction rate, indicating that limitation of the reaction by gas diffusion in the boundary layer can be neglected⁴. Thus, the kinetic study was accomplished under reducing gas flow rate of 150 mL/min. The reduction test also demonstrated a higher reduction rate at 700 °C owing to the reduction of hematite (Fe_2O_3) to magnetite (Fe_3O_4)³³. Figure 10b shows that the increase in diameter of the pellet decreases the reaction rate, suggesting that mass transfer in the pores hinders the reduction of iron-ore pellets and that the diffusion mechanism influences the pellet reduction process^{33,34}. However, at the start of reduction, pellet diameter has a weaker effect on the reduction, thereby suggesting the participation of other mechanisms besides diffusion.

The first step of the kinetic investigation was the comparison of the linear trends (R^2) of the relationship of da/dt vs. $f(\alpha)$. Functions that exceeded 0.9 ($R^2 \geq 0.9$) were accepted as possible mechanism controllers (Table 4). Table 6 shows that all functions exhibit a high linear trend ($R^2 \geq 0.9$) for $\ln da/dt$ vs. $\ln f(\alpha)$ for all temperatures analyzed, indicating that

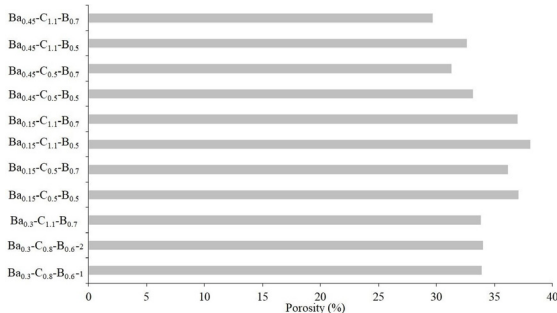


Figure 8. Influence of composition on pellet porosity.

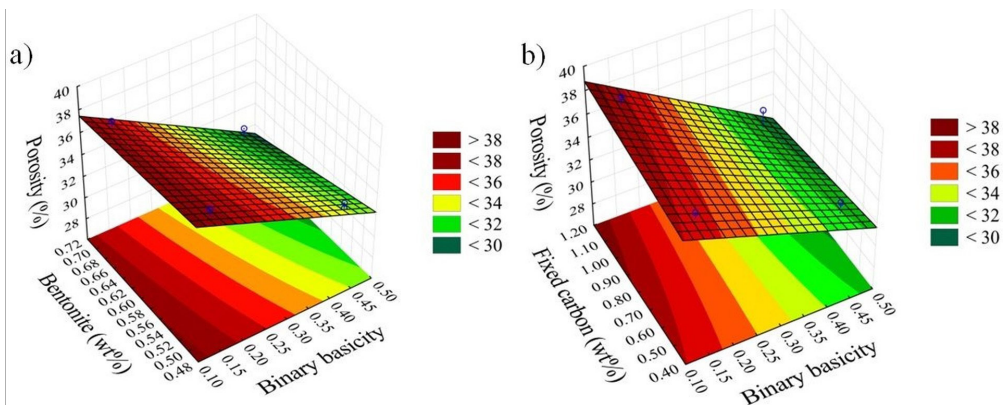


Figure 9. Response surface plot. a) Relation between porosity against bentonite and binary basicity. b) Relation between porosity against fixed carbon and binary basicity.

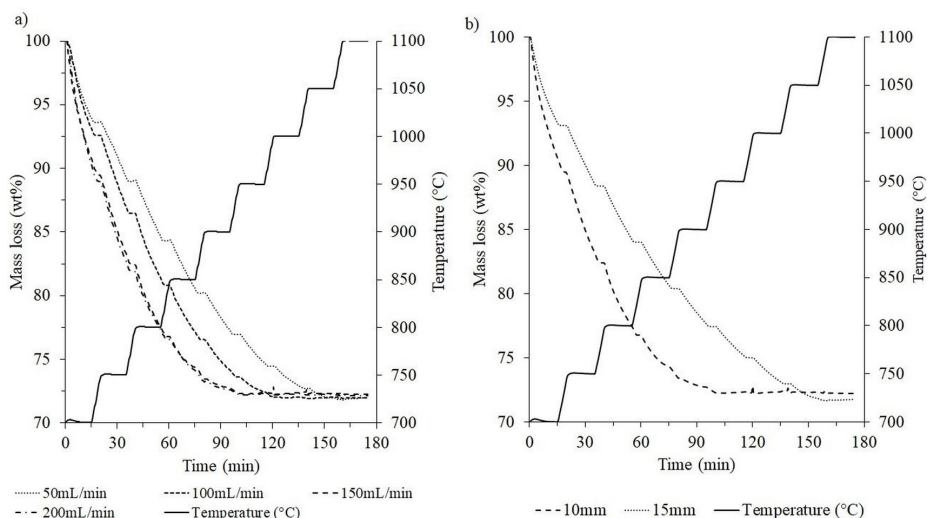


Figure 10. Thermogravimetric tests. a) Influence of CO flow on the reduction of the iron-ore pellet; b) influence of pellet diameter on the reduction reaction.

Table 6. Linear trend (R^2) of the relationship between $\ln d\alpha/dt$ vs. $\ln f(\alpha)$ for the kinetic models for gas–solid reaction presented in Table 3 for each investigated temperature.

Temperature (°C)	Controller mechanisms							
	R2	R3	D1	D2	D3	D4	A2	A3
700	0.96	0.96	0.93	0.93	0.93	0.93	0.90	0.93
750	0.99	0.99	0.98	0.98	0.98	0.98	0.99	0.94
800	0.93	0.93	0.95	0.95	0.95	0.95	0.90	0.87
850	0.96	0.96	0.96	0.96	0.96	0.96	0.97	0.97
900	0.90	0.89	0.88	0.91	0.90	0.90	0.90	0.90

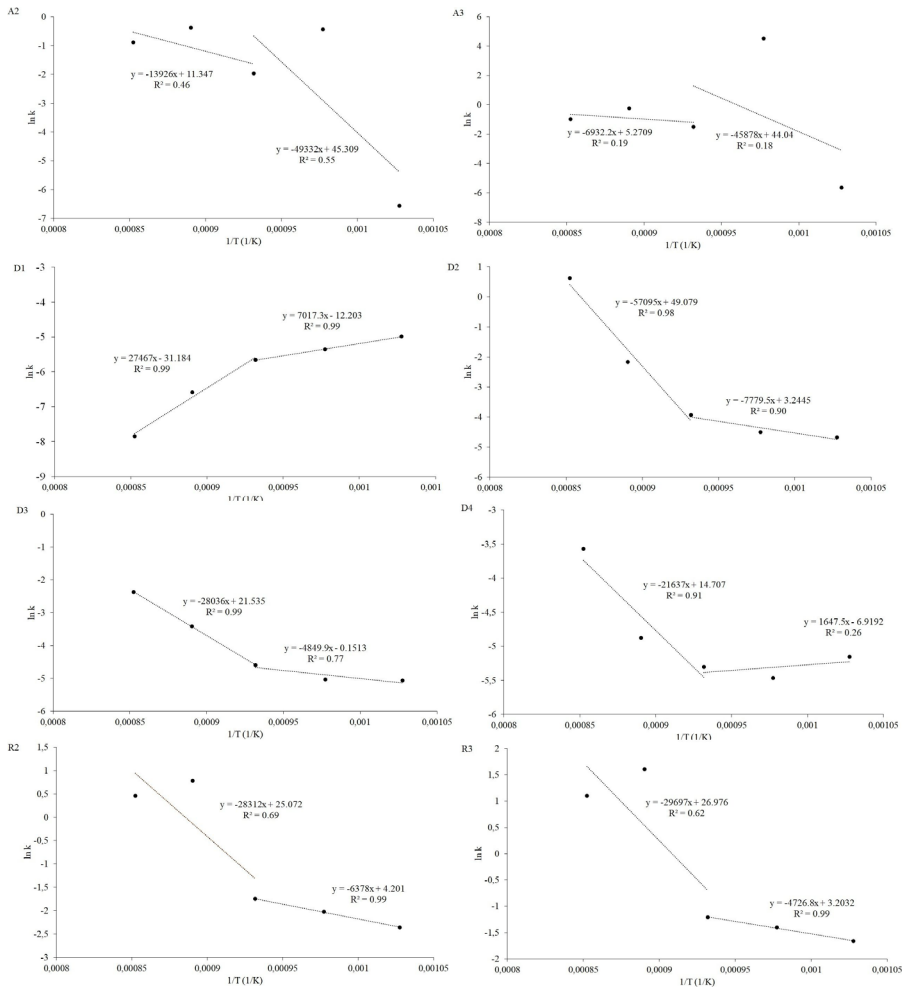


Figure 11. Arrhenius plots of the reduction of the iron-ore pellet containing lime sludge under CO atmosphere.

all models can be validated. The second step of the kinetic investigation was obtaining the Arrhenius plots for all kinetic models (Figure 11). One initial assumption was that the controller mechanism did not change during the reduction reaction. However, the Arrhenius plots were not linear ($R^2 < 0.9$), indicating a change in the controller mechanism during the reduction reaction. The second hypothesis was that a possible change in the controlling mechanism occurred during the reduction reaction. The Arrhenius plots were

split into two steps (700–800 °C and 800–900 °C). A linear trend higher than 0.9 ($R^2 > 0.9$) was reached as seen in Figure 11, indicating a change in controller mechanism during reduction. At temperatures less than 800 °C, functions R2, R3, and D2 presented linear trends ($R^2 \geq 0.9$), indicating a combination of controller mechanisms between chemical reaction and diffusion. Kinetic models with low linearity ($R^2 < 0.9$) do not follow the Arrhenius law; therefore, they do not follow the proposed kinetic model. The E_a value

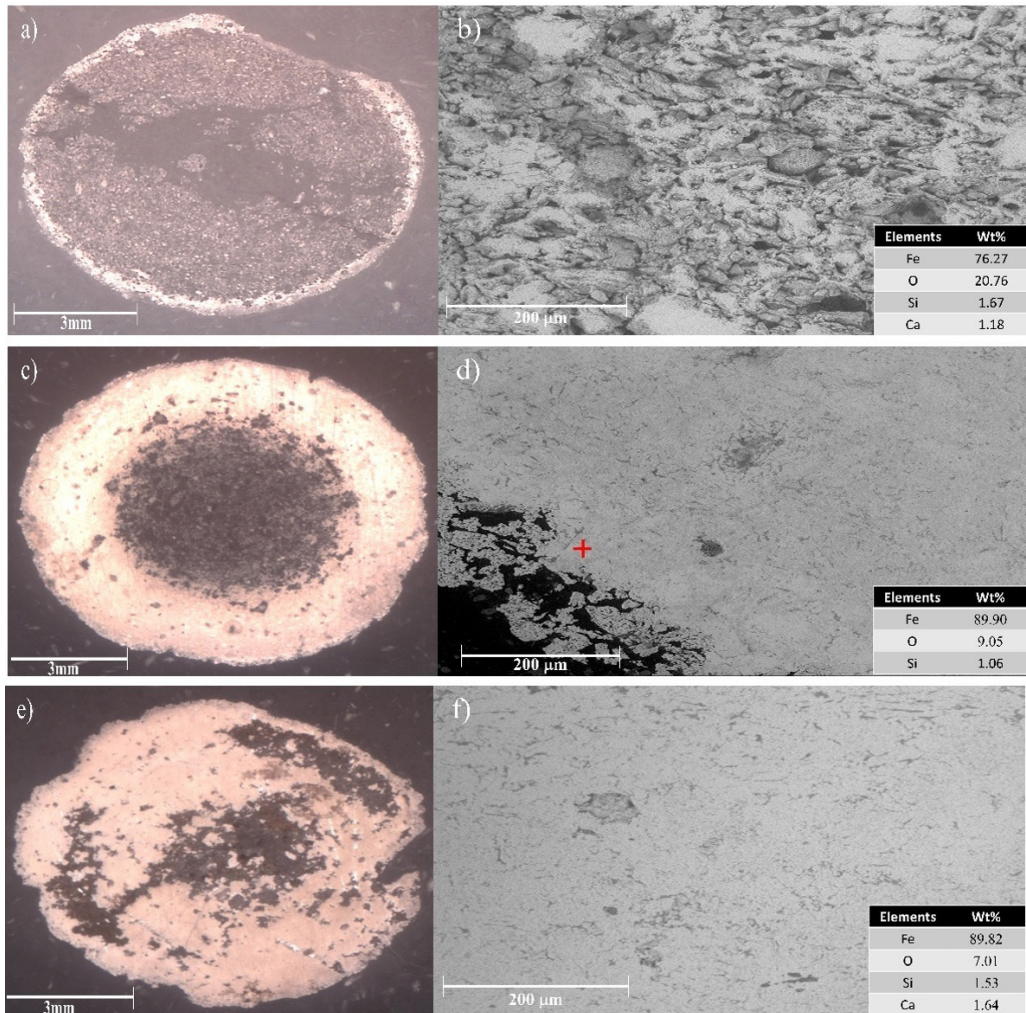


Figure 12. a) Optical microscopy at the end of the 700 °C isotherm; b) SEM image at the end of the 700 °C isotherm; c) optical microscopy image at the end of the 800 °C isotherm; d) SEM image at the end of the 800 °C isotherm; e) optical microscopy image at the end of the reduction reaction; and f) SEM image at the end of the reduction reaction.

up to 800 °C ranged between 39.3 and 64.68 kJ/mol. Functions D2, D3, and D4 reached linearity ($R^2 \geq 0.9$) at temperatures exceeding 800 °C, suggesting that only the diffusion as the only controller mechanism, with an E_a range of 179.89–233.10 kJ/mol.

Figure 12a shows that the pellet underwent reduction up to 700 °C and started to form a layer of reduced iron around the unreacted core. The SEM image of the reduced layer and EDS X-ray spectrum (Figure 12b) shows a porous structure containing iron (76.27 wt%) and oxygen (20.76 wt%), which suggest the presence of iron oxides and/or iron. The XRD analysis (Figure 13a) shows the iron-ore pellet reduced up to 700 °C and contained magnetite, wustite, and metallic iron, indicating that reduction reactions occurred in consecutive steps according to Equation 7³⁵. In addition, the absence of the hematite peak in Figure 13a implies a rapid reduction to magnetite, as previously mentioned. In addition, the wustite peak showed the highest intensity in Figure 13a, indicating that the first step is controlled by the rapid reduction of hematite

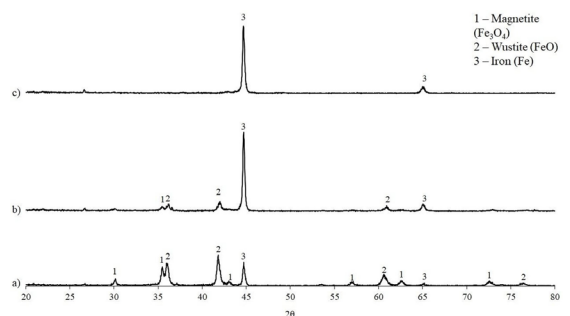
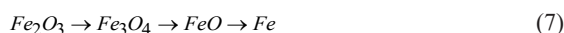


Figure 13. XRD spectra of the iron-ore pellets reduced in different isotherms: a) at the end of the 700 °C isotherm; b) at end of the 800 °C isotherm; and c) at the end of the reduction reaction.

to wustite⁹. According to Ponomar et al.³³, the reduction of hematite to magnetite is accompanied by the conversion of a rhombohedral system to a cubic crystal system followed by a

volumetric variation, which is responsible for the formation of micropores on the magnetite surface. The formation of these defects contributes to the higher reduction rate into the first step, facilitating the penetration of the reducing gas into the unreacted grains of the pellet.



According to Li^{36} , the initial reduction stage of a porous solid occurs on the surface of the pores. Therefore, the formation of micropores due to reduction of hematite to magnetite contributes to increased porosity, which facilitates gaseous diffusion. As the reduction of magnetite to wustite proceeded, the reacted layer around the unreacted core increased, hampering the diffusion of CO into the pellet^{9,22}. At 800 °C (Figure 12c) the reduced layer advances toward the interior of the pellet. Figure 12d shows that the iron-ore pellet reduced up to 800 °C presents a dense outer layer composed of 89.9 wt% iron and 9.05 wt% oxygen from wustite and/or iron (Figure 12b). The formation of the dense iron layer decreases the porosity and hinders the diffusion of the reducing gas into the pellet, thereby decreasing the reaction rate and increasing the E_a of reduction^{35,37}.

Figure 12e shows the pellet after the reduction process (at 1100 °C), in which the unreacted core has disappeared. Figure 12f shows the formation of dense iron with 95.3 wt% Fe and 4.7 wt% of oxygen. Figure 13c displays only peaks of iron and SiO_2 , which demonstrate the complete reduction of iron oxide in the iron-ore pellet.

4. Conclusions

This study demonstrates that lime sludge offers considerable potential for application as fluxing material in the pelleting process of iron ore. The optimal composition of the iron-ore pellet includes a binary basicity of 0.45 and percentages of fixed carbon of 0.5% and bentonite of 0.7%. Such composition achieved test results of 3.6 drops/pellet, tumble test values of 1.57 wt%, dry-pellet mechanical strength of 3.2 kgf/pellet, fired-pellet mechanical strength of 214.83 kgf/pellet, and a porosity of 31.28%. The kinetic investigation shows that the use of lime sludge does not influence the reduction reaction of the iron-ore pellets. Reduction occurs in two steps: the first step occurs in the temperature range of 700–800 °C, with E_a ranging between 39.3 and 64.68 kJ/mol and controller mechanism being a mixture of chemical reaction and diffusion. The second step is in the temperature range of 800–900 °C, in which the reaction is controlled by the diffusion of the reducing gas into the pellet, with E_a ranging between 179.89 and 233.10 kJ/mol.

Herein, the generated lime sludge in Brazil was estimated to be approximately 16.8 million tons: to produce 1 kg of pellets with a binary basicity of 0.45 (by adopting the chemical compositions of inputs used in this study), 19 g of lime sludge is required; consequently, 884.2 million tons iron-ore pellets can be produced using the amount of generated lime sludge. Therefore, a regenerative model between the mineral/ironmaking/pulp and paper industries can be developed. In addition, the substitution of limestone with lime sludge can decrease both the need to extract finite mineral resources and required areas for lime sludge disposal.

5. Acknowledgements

The authors would like to thank Coordenação de Aperfeiçoamento de Pessoal de Nível Superior – Brazil and University of Extremo Sul Catarinense.

6. References

- Rath SS, Rao DS, Tripathy SK, Biswal SK. Characterization vis-à-vis utilization of blast furnace flue dust in the roast reduction of banded iron ore. *Process Saf Environ Prot.* 2018;117:232-44. <http://dx.doi.org/10.1016/J.PSEP.2018.05.007>.
- Najafabadi AHM, Masoumi A, Vaez-Allaei SM. Analysis of abrasive damage of iron ore pellets. *Powder Technol.* 2018;331:20-7. <http://dx.doi.org/10.1016/J.POWTEC.2018.02.030>.
- Cavalcanti PP, Tavares LM. Statistical analysis of fracture characteristics of industrial iron ore pellets. *Powder Technol.* 2018;325:659-68. <http://dx.doi.org/10.1016/J.POWTEC.2017.11.062>.
- Santos FE, Borgert CH, Rosso L No, Oliveira JR, Ferreira HJ Fo, Alves JO et al. Physical characterization and kinetic analysis of the iron ore pellets produced with marble waste. *Metall Mater Trans B.* 2021;52:1664-80. <http://dx.doi.org/10.1007/s11663-021-02131-8>.
- Fadel I, Werner A, Rocha M, Bassil S. Produção e vendas da Vale no 1T21 [Internet]. Rio de Janeiro: Vale; 2021. p. 1-18 [cited 2022 Dec 15]. Available from: <https://www.vale.com/pt/comunicados-resultados-apresentacoes-e-relatorios>
- Fadel I, Werner A, Rocha M, Bassil S. Produção e vendas da Vale no 2T20 [Internet]. Rio de Janeiro: Vale; 2020. p. 1-19 [cited 2022 Dec 15]. Available from: <https://www.vale.com/pt/comunicados-resultados-apresentacoes-e-relatoriof>
- Fadel I, Werner A, Rocha M, Bassil S. Produção e vendas da Vale no 3T20 [Internet]. Rio de Janeiro: Vale; 2020. p. 1-15 [cited 2022 Dec 15]. Available from: <https://api.mziq.com/mzfilemanager/v2/d/53207d1c-63b4-48f1-96b7-19869fae19fe/bc991cb6-b11f-4c3c-85b5-773acfd067a7?origin=1>
- Norouzi M, Châfer M, Cabeza LF, Jiménez L, Boer D. Circular economy in the building and construction sector: a scientific evolution analysis. *J Build Eng.* 2021;44:102704. <http://dx.doi.org/10.1016/J.JOBE.2021.102704>.
- Dishwar RK, Sinha OP. Effect of basicity on the activation energy during reduction of highly fluxed iron ore pellets. *Fuel.* 2021;296:120640. <http://dx.doi.org/10.1016/J.FUEL.2021.120640>.
- IBÁ: Indústria Brasileira de Árvores [homepage on the Internet]. Brasília: IBÁ; c2020; [cited 2022 Dec 15]. Available from: <https://www.iba.org/historico-de-desempenho>
- Vashistha P, Kumar V, Singh SK, Dutt D, Tomar G, Yadav P. Valorization of paper mill lime sludge via application in building construction materials: a review. *Constr Build Mater.* 2019;211:371-82. <http://dx.doi.org/10.1016/J.CONBUILDMAT.2019.03.085>.
- Phanikumar BR, Raju ER. Compaction and strength characteristics of an expansive clay stabilised with lime sludge and cement. *Soil Found.* 2020;60(1):129-38. <http://dx.doi.org/10.1016/J.SANDE.2020.01.007>.
- Singh SK, Singh A, Singh B, Vashistha P. Application of thermo-chemically activated lime sludge in production of sustainable low clinker cementitious binders. *J Clean Prod.* 2020;264:121570. <http://dx.doi.org/10.1016/j.jclepro.2020.121570>.
- Guo Y, Liu K, Chen F, Wang S, Zheng F, Yang L et al. Effect of basicity on the reduction swelling behavior and mechanism of limestone fluxed iron ore pellets. *Powder Technol.* 2021;393:291-300. <http://dx.doi.org/10.1016/J.POWTEC.2021.07.057>.
- Umadevi T, Kumar P, Lobo NF, Prabhu M, Mahapatra PC, Ranjan M. Influence of pellet basicity (CaO/SiO₂) on iron ore pellet properties and microstructure. *ISIJ Int.* 2011;51(1):14-20. <http://dx.doi.org/10.2355/isijinternational.51.14>.
- ISO: International Organization for Standardization. ISO 3271:2015: determination of the tumble and abrasion indices

- [Internet]. Geneva: ISO; 2015 [cited 2022 Oct 14]. Available from: <https://www.iso.org/standard/62135.html>
17. ISO: International Organization for Standardization. ISO 4700:2015: determination of the crushing strength [Internet]. Geneva: ISO; 2015 [cited 2022 Oct 14]. Available from: <https://www.iso.org/standard/62146.html>
 18. Roduit B, Maciejewski M, Baiker A. Influence of experimental conditions on the kinetic parameters of gas-solid reactions - parametric sensitivity of thermal analysis. *Thermochim Acta*. 1996;282-283(Spe):101-19. [http://dx.doi.org/10.1016/0040-6031\(96\)02882-1](http://dx.doi.org/10.1016/0040-6031(96)02882-1).
 19. Khawam A, Flanagan DR. Solid-state kinetic models: basics and mathematical fundamentals. *J Phys Chem B*. 2006;110(35):17315-28.
 20. Chen F, Sørensen O, Meng G, Peng D. Thermal decomposition of BaC₂O₄·0.5H₂O studied by stepwise isothermal analysis and non-isothermal thermogravimetry. *J Therm Anal*. 1998;53:397-410.
 21. Pineau A, Kanari N, Gaballah I. Kinetics of reduction of iron oxides by H₂. Part II. Low temperature reduction of magnetite. *Thermochim Acta*. 2007;456(2):75-88. <http://dx.doi.org/10.1016/j.tca.2007.01.014>.
 22. Pineau A, Kanari N, Gaballah I. Kinetics of reduction of iron oxides by H₂. Part I: low temperature reduction of hematite. *Thermochim Acta*. 2006;447(1):89-100. <http://dx.doi.org/10.1016/j.tca.2005.10.004>.
 23. Sohn I, Jung SM. Effect of metal additions to the reduction of iron oxide composite pellets with hydrogen at moderate temperatures. *Steel Res Int*. 2011;82(12):1345-54. <http://dx.doi.org/10.1002/srin.201100144>.
 24. Sivrikaya O, Arol AI. The bonding/strengthening mechanism of colemanite added organic binders in iron ore pelletization. *Int J Miner Process*. 2012;110-111:90-100. <http://dx.doi.org/10.1016/j.minpro.2012.04.010>.
 25. Forsmo S. Influence of green pellet properties on pelletizing of magnetite iron ore [thesis]. Luleå: Luleå University of Technology; 2014.
 26. Prusti P, Barik K, Dash N, Biswal SK, Meikap BC. Effect of limestone and dolomite flux on the quality of pellets using high LOI iron ore. *Powder Technol*. 2021;379:154-64. <https://doi.org/10.1016/j.powtec.2020.10.063>.
 27. Abouzeid AZM, Kotb IM, Negm AA. Iron ore fluxed pellets and their physical properties. *Powder Technol*. 1985;42(3):225-30. [http://dx.doi.org/10.1016/0032-5910\(85\)80057-7](http://dx.doi.org/10.1016/0032-5910(85)80057-7).
 28. Dwarapudi S, Ghosh TK, Shankar A, Tathavadkar V, Bhattacharjee D, Venugopal R. Effect of pellet basicity and MgO content on the quality and microstructure of hematite pellets. *Int J Miner Process*. 2011;99(1-4):43-53. <http://dx.doi.org/10.1016/j.minpro.2011.03.004>.
 29. Silva BB, Cunha ER, Carvalho RM, Tavares LM. Modeling and simulation of green iron ore pellet classification in a single deck roller screen using the discrete element method. *Powder Technol*. 2018;332:359-70. <http://dx.doi.org/10.1016/j.powtec.2018.04.005>.
 30. Prasad R, Gupta K, Poras A, Agarwal S. Microstructure and phase analysis of indurated iron ore pellets. *Mater Today Proc*. 2019;26(2):2636-42. <https://doi.org/10.1016/j.matpr.2020.02.556>.
 31. Meng X, Shi L, Yao L, Zhang Y, Cui L. Fe (III) clusters modified Bi₂O₃/TiO₂ nanosheets photocatalyst for boosting photocatalytic performance through interfacial charge transfer effect. *Colloids Surf A: Physicochem Eng Asp*. 2020;594:124658. <http://dx.doi.org/10.1016/j.colsurfa.2020.124658>.
 32. Praes GE, Arruda JD, Lemos LR, Tavares RP. Assessment of iron ore pellets production using two charcoals with different content of materials volatile replacing partially anthracite fines. *J Mater Res Technol*. 2019;8(1):1150-60. <https://doi.org/10.1016/j.jmrt.2018.09.003>.
 33. Ponomar VP, Brik OB, Cherevko YI, Ovsienko VV. Kinetics of hematite to magnetite transformation by gaseous reduction at low concentration of carbon monoxide. *Chem Eng Res Des*. 2019;148:393-402. <http://dx.doi.org/10.1016/j.cherd.2019.06.019>.
 34. Junca E, Grillo FF, Restivo TAG, Oliveira JR, Espinosa DCR, Tenório JAS. Kinetic investigation of synthetic zinc ferrite reduction by hydrogen. *J Therm Anal Calorim*. 2017;129(2):1215-23. <http://dx.doi.org/10.1007/s10973-017-6222-7>.
 35. Yu D, Zhu M, Utigard TA, Barati M. TG/DTA study on the carbon monoxide and graphite thermal reduction of a high-grade iron nickel oxide residue with the presence of siliceous gangue. *Thermochim Acta*. 2014;575:1-11. <http://dx.doi.org/10.1016/j.tca.2013.10.015>.
 36. Li Z. General rate equation theory for gas-solid reaction kinetics and its application to CaO carbonation. *Chem Eng Sci*. 2020;227:115902. <http://dx.doi.org/10.1016/J.CES.2020.115902>.
 37. He K, Zheng Z, Chen Z, Chen H, Hao W. Kinetics of hydrogen reduction of Brazilian hematite in a micro-fluidized bed. *Int J Hydrogen Energy*. 2021;46(5):4592-605. <http://dx.doi.org/10.1016/j.ijhydene.2020.10.263>.